JOURNAL OF SPACECRAFT AND ROCKETS
Vol. 41, No. 4, July–August 2004

# Catalytic Atom Recombination on $ZrB_2$/SiC and $HfB_2$/SiC Ultrahigh-Temperature Ceramic Composites

Jochen Marschall*
*SRI International, Menlo Park, California 94025*
Adam Chamberlain†
*University of Missouri–Rolla, Rolla, Missouri 65409*
and
Daniel Crunkleton‡ and Bridget Rogers§
*Vanderbilt University, Nashville, Tennessee 37235*

**Results are presented of an experimental investigation into the efficiency of zirconium diboride/silicon carbide and hafnium diboride/silicon carbide ultrahigh-temperature ceramic composites for catalyzing the surface recombination of dissociated oxygen and nitrogen at moderate surface temperatures. Experiments were conducted with a diffusion-tube side-arm reactor, together with laser-induced fluorescence species detection diagnostics. Experiments reveal recombination coefficients in the range between silica glasses and oxidized metals, as well as evidence of environment-induced surface modification.**

## Introduction

ULTRAHIGH temperature ceramic (UHTC) composites based on zirconium diboride ($ZrB_2$) and hafnium diboride ($HfB_2$) are promising materials for use as sharp leading-edge components on hypersonic flight vehicles. Both the diborides and their primary metal oxides have extremely high melting points.[1] UHTC composites have shown good dimensional stability in low-pressure supersonic aerothermal heating environments, where other refractory materials rapidly fail by melting, spalling, pyrolyzing, or ablating.[2] Several studies have demonstrated that the high-temperature oxidation/ablation resistance of diboride-based UHTC materials is enhanced by the addition of silicon carbide (SiC).[3–7] Two promising formulations are known as A-7, with a nominal composition of $HfB_2$ with 20-vol% SiC and A-8, with a nominal composition of $ZrB_2$ with 20-vol% SiC. These formulations were flown during the slender hypervelocity aerothermodynamic research probe flight experiments, SHARP B1[8,9] and SHARP B2. (Details of the SHARP B1 and B2 flight experiments are available at http://asm.arc.nasa.gov/.)

One aspect of UHTC performance not previously investigated is the catalytic efficiency of $ZrB_2$/SiC and $HfB_2$/SiC composites for recombining dissociated oxygen and nitrogen. During hypersonic flight through Earth's atmosphere, high-temperature shock waves form in front of vehicle leading edges. Molecular oxygen and nitrogen, with respective dissociation energies of approximately 5.2 eV (500 kJ/mol) and 9.8 eV (950 kJ/mol), can dissociate in these extreme environments. If the resulting atomic species diffuse to the vehicle surface and recombine there, this dissociation energy becomes available, and some fraction may go directly to the surface as heat. The importance of surface catalyzed reactions to Earth entry heating has been demonstrated in a series of flight experiments on NASA's Space Shuttle Orbiter.[10–12]

Received 13 June 2003; revision received 16 September 2003; accepted for publication 7 October 2003. 

*Research Scientist, Molecular Physics Laboratory; jochen.marschall@sri.com. Senior Member AIAA.
†Graduate Student, Department of Ceramics Engineering.
‡Assistant Professor, Department of Chemical Engineering.
§Postgraduate Researcher, Department of Chemical Engineering.

Many studies of oxygen and nitrogen recombination have been done on a variety of different structural and thermal protection system materials. However, no experimental data exist for UHTC materials or their oxides. UHTC materials are intermetallic compounds with unique chemical and electrical properties; their catalytic performance may differ substantially from those of pure metals or pure ceramics that have been tested in the past. It is also evident that the catalytic behavior of UHTC materials under transient, high-temperature plasma exposures must be closely coupled with development of oxide layers. Generally, metals have been found to catalyze oxygen and nitrogen recombination much more efficiently than ceramics. It is believed that the catalytic efficiency of a material is related to its intrinsic electronic transport properties. In their virgin state, UHTC composites have an electrical resistivity of ~10–20 $\mu\Omega \cdot$ cm at room temperature, a range comparable to that of many iron alloys. As in metals, the resistivity of virgin UHTC materials increases linearly with increasing temperature. However, once a surface oxide forms, this metal-like behavior will change. $B_2O_3$ and $SiO_2$ are covalently bonded insulators, and $ZrO_2$ and $HfO_2$ are ionic compounds. The intrinsic electrical conductivity of these materials is much less than that of the virgin UHTC materials. The electrical transport mechanisms are also different. In the case of $B_2O_3$ and $SiO_2$, semiconductorlike transport is generated by impurities that can create $p$- or $n$-type doping, whereas for $ZrO_2$ and $HfO_2$, electrical conductivity is dominated by oxygen ion diffusion. It appears that oxygen recombination is more favorable on $p$-type semiconducting surfaces.[13,14] The $n$- or $p$-type nature of the amorphous silica and boron oxides in UHTC oxide layers has not been experimentally determined, and no data on oxygen or nitrogen recombination on $ZrO_2$ or $HfO_2$ surfaces were found in the literature.

Here, we present the results of a first experimental investigation into the efficiency of $ZrB_2$/SiC and $HfB_2$/SiC composites for catalyzing the recombination of dissociated oxygen and nitrogen. The present study is focused on a moderate temperature regime (from room temperature to 1000 K) that can be accessed by the use of a diffusion-tube side-arm reactor technique. We find recombination efficiencies that lie in the range between silica glasses and oxidized metals, as well as evidence of environment-induced oxidation that modifies the catalytic efficiency.

## Materials and Methods

### Side-Arm Reactor Facility

Surface catalysis experiments were conducted in a diffusion-tube side-arm reactor. The theory of surface catalysis measurements in

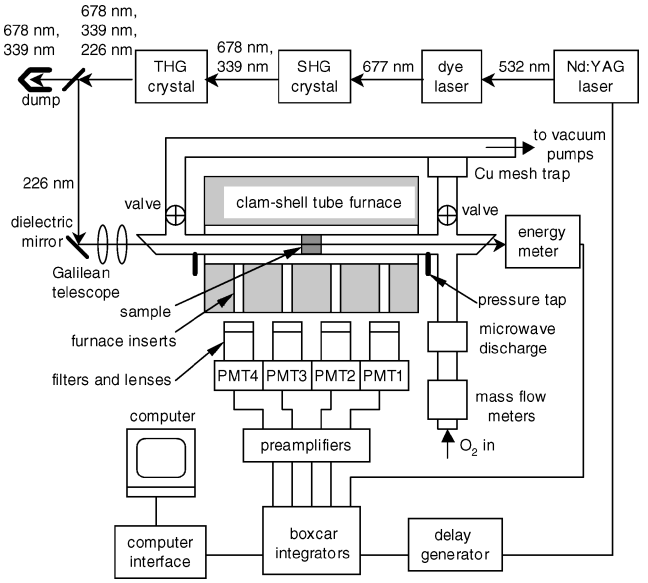


**Fig. 1 Diagram of diffusion-tube side-arm reactor facility.**

a diffusion-tube side-arm reactor, as well as the side-arm reactor facility, has been described in a number of publications.[15–17] Here we give only a brief overview of the equipment and test procedures. A diagram of the facility is shown in Fig. 1.

The reactor consists of a Pyrex® main flow tube and a quartz deadend side-arm tube attached via a cross. A 46-cm length of the side-arm tube was enclosed in a clam-shell tube furnace capable of reaching ~1500 K. Molecular gases are introduced into the upstream side of the flow tube and exhausted downstream with a turbomolecular pump backed with a roughing pump. A microwave cavity positioned upstream of the cross was used to dissociate a fraction of the molecular gas to produce either O or N atoms. As the atomic species diffuse down the side-arm tube, they recombine on the walls. Under steady-state conditions, a decaying atom concentration profile is established along the axis of the side-arm tube. The shape of this profile is determined by the catalytic activity of the reactor walls. Their catalytic efficiency is parameterized by the recombination coefficient $\gamma$, defined as the fraction of atomic collisions with the surface that remove an atom from the gas phase. Recombination coefficients are determined by matching measured atom concentration profiles to numerical solutions of the appropriate reaction–diffusion equation.[15,18,19]

Measurements of the (relative) atom concentration are made as a function of axial position along the side-arm tube using two-photon laser-induced fluorescence (LIF). In this process, atoms are excited with two photons of ultraviolet light and monitored by their subsequent fluorescence in the near infrared. Ultraviolet (UV) light, at wavelengths of ~226 nm for two-photon O-atom excitation and ~207 nm for two-photon N-atom excitation, is generated by frequency tripling red light produced by a Continuum ND60 dye laser. Frequency tripling is achieved using two beta-barium borate crystals for second and third harmonic generation. Red light at ~678 nm is produced using LDS 698 laser dye, and red light at ~621 nm is produced using Rhodamine 640 laser dye; both dyes are dissolved in methanol. The dye laser is pumped with the frequency-doubled output (~532 nm green light) from a Continuum NY81 Nd:YAG laser.

The UV laser light is directed through a collimating Galilean telescope and then through a quartz Brewster angle window down the centerline of the side-arm tube by the use of dichroic mirrors. A Molectron energy meter is used to monitor fluctuations in the laser pulse energy as the beam exits the side-arm tube through a second Brewster angle window on the cross. Atom fluorescence is monitored at right angles to the side-arm tube through quartz-lined optical access ports in the furnace by the use of four gated Hamamatsu R636 photomultiplier (PMT) tubes spaced ~8.9 cm apart. The PMTs are fitted with narrow-band interference filters, with a bandwidth of ~3 nm, centered at 845 nm for O-atom fluorescence and 745 nm for N-atom fluorescence. Signals from the energy meter and the PMTs were sent to a Stanford Research Systems data acquisition system consisting of a preamplifier, several boxcar integrators, and a computer interface module. The laser and data acquisitions system were synchronized at 10 Hz by the use of a Stanford Research Systems delay generator.

#### Surface Catalysis Test Samples

UHTC billets were provided by the NASA Ames Research Center, from material stock manufactured during the SHARP B1 and B2 programs. The as-pressed cylindrical billets were ~7.6 cm in height and ~7.6 cm in diameter. Catalysis test samples, in the form of 2.1-cm-long tubes with an outer diameter of 2.0 cm and a wall thickness of 0.28 cm were machined from a single disk cut from each billet. The test samples where machined by the use of techniques similar to those employed in the manufacture of SHARP B1 and SHARP B2 flight components. Electrical discharge machining (EDM) was used to cut the disks from the billets and the tubes out of the disks. Diamond grinding of the inner tube surfaces was used to achieve final dimensions.

After machining, the samples were rinsed with methanol, cleaned in an ultrasonic bath for ~15 min in a water–detergent mixture, rinsed in distilled water, and then air dried. After being loaded into the side-arm reactor, samples were conditioned under vacuum for at least 12 h before testing. This was done to remove residual, loosely bound volatiles from surfaces without heating and to provide a uniform initial condition for all experiments. In actual application, UHTC materials may be subjected to a variety of environmental contaminates, for example, water, salts, and hydrocarbons, the ramifications of which must be addressed in separate experiments.

## Surface Catalysis Measurements

Three types of measurements were done as part of the UHTC surface catalysis experiments. First, the relative signal response of the four PMTs was determined by turning the diffusion tube into a flow tube. Under flow tube conditions, wall losses are minimized and each PMT should see fluorescence from similar atom concentrations. With small corrections for concentration differences due to surface recombination and pressure gradients, as well as the pressure dependence of the fluorescence yield, the relative sensitivity of each PMT can be determined and used to normalize diffusion tube data. Second, diffusion tube measurements were made to determine the recombination coefficients of quartz tube inserts. These data were analyzed with a classic exponential decay model.[18] Third, diffusion tube experiments were made to determine the recombination coefficients of UHTC samples. UHTC samples were placed within the quartz tube inserts and positioned at the midpoint of the furnace-enclosed side-arm tube. A three-section diffusion tube model was used to extract recombination coefficients from the measured data.[15] In this model, the recombination coefficients of the first and third tube sections were fixed at the measured quartz values, and the tube diameter was fixed at the quartz tube insert value.

Surface catalysis testing proceeded in a cyclical manner. Before and after each UHTC sample was tested, the LIF signal normalization was confirmed through flow-tube measurements and the recombination coefficients of the quartz sample tubes were measured as a function of temperature in diffusion tube experiments. Each UHTC sample was tested on three different days, at several discreet temperatures, with multiple measurements at each temperature. During the first test run, measurements were made at 295, 473, and 673 K; during the second test run these measurements were repeated and extended to 923 K; and during the third test run these measurements were repeated once more. The reactor was not opened between runs, and the samples remained continuously under vacuum.

#### Surface Analysis Samples

The UHTC samples used for catalysis testing are not easily probed by surface analysis techniques because of their tubular shape. A second set of samples was prepared in the form of ~1-cm$^2$ squares

**Table 1 Test conditions seen by the 10 A-7 and A-8 UHTC surface analysis specimens**

| Gas environment | Run 1[a] | Run 2[b] |
|---|---|---|
| Vacuum | 1,2 | 2 |
| 300 mtorr oxygen (discharge off) | 3,4 | 4 |
| 300 mtorr oxygen (discharge on) | 5,6 | 6 |
| 300 mtorr nitrogen (discharge off) | 7,8 | 8 |
| 300 mtorr nitrogen (discharge on) | 9,10 | 10 |

[a]Ramp to 673 K, hold 4 h, cool under vacuum.
[b]Ramp to 673 K, hold 2 h, ramp to 923 K, hold 2 h, cool under vacuum.

from scrap material remaining from the manufacture of the catalysis samples. These scraps were thin (~2–4 mm thick) cross sections of material cut by EDM directly adjacent to the catalysis sample disks within the billets. The faces nearest the catalysis sample disks were polished to a mirror finish with diamond grit, and individual coupons were cut from the polished cross sections with a diamond cutting wheel. At least 12 samples of each UHTC composition were obtained in this way. The samples were rinsed with methanol, cleaned in an ultrasonic bath, and air dried before insertion into the side-arm reactor.

#### Surface Analysis Sample Exposures

The surface analysis samples were positioned with their polished side facing up in the side-arm tube at the same nominal location as the catalysis samples and exposed to a variety of gas and heating conditions (Table 1). During run 1 heating cycles, two samples at a time were heated to 673 K, held for 4 h at temperature, and then cooled under vacuum. After cooling, one of the samples was removed. The remaining sample was exposed to the run 2 heating cycle, which consisted of heating to 673 K, holding at temperature for 2 h, heating to 923 K, holding at temperature for 2 h, and then cooling under vacuum. These heating cycles are similar to those seen by the surface catalysis samples, though not identical. After exposure, samples were stored at ambient temperature and atmospheric conditions until surface analysis. Several additional samples were left untested to serve as unexposed standards for comparison.

#### Surface Analyses

Samples were examined with energy dispersive x-ray (EDX) analysis and x-ray photoelectron spectroscopy (XPS). The EDX analyses were performed with a LEO-435VP scanning electron microscope operated at 20 kV, with an Oxford EDX system fit with a SiLi detector. XPS analyses were performed in a hemispherical analyzer-based system (Leybold-Heraeus, LH 18) with Al $K_\alpha$ (1486.6 eV) x rays and a 45-deg takeoff angle.

The EDX technique samples material to a depth of several micrometers with a lateral resolution of several 100 $\mu$m. The XPS technique probes only near-surface material to a depth of several nanometers with lateral resolution of ~1 mm.

## Results

The results of the side-arm reactor experiments are the measured recombination coefficients shown in Figs. 2–6. The averaged recombination coefficient values for the quartz sample tubes are also included in the Figs. 2, 3, 5, and 6 for comparison to the UHTC values. The melting point $T_m$ of crystalline $B_2O_3$ is indicated in each of Figs. 2, 3, 5, and 6. Its significance will be discussed in the Discussion section. The data demonstrate an interesting, history-dependent behavior that suggests that UHTC surfaces are modified during testing.

#### Oxygen Surface Recombination

The measured oxygen recombination coefficients for the A-8 and A-7 materials are shown in Figs. 2 and 3, respectively. The following behavior is observed for the $ZrB_2$, 20-vol% SiC sample in Fig. 2. During the first test, recombination coefficients of ~$1 \times 10^{-3}$–$2 \times 10^{-3}$ are found at room temperature. On heating to

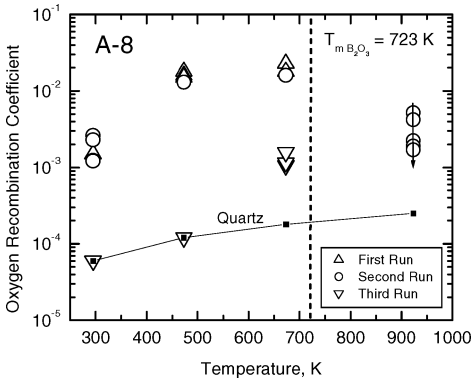


**Fig. 2 Oxygen recombination coefficient of A-8 ($ZrB_2$, 20-vol% SiC) UHTC specimen.**

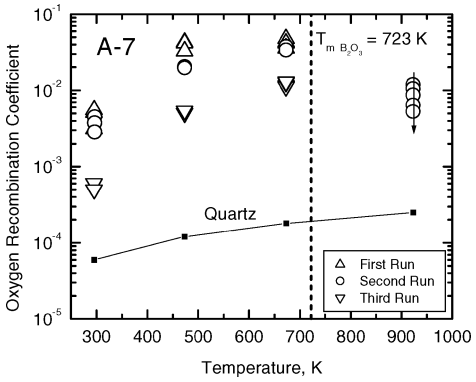


**Fig. 3 Oxygen recombination coefficient of A-7 ($HfB_2$, 20-vol% SiC) UHTC specimen.**

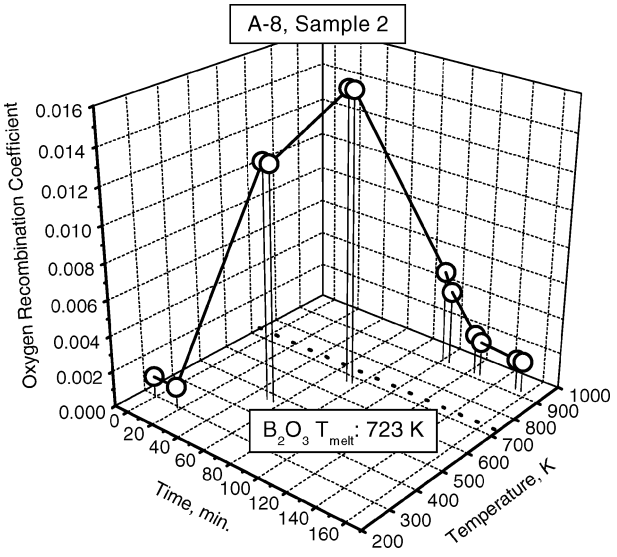


**Fig. 4 Measured oxygen recombination coefficients for the A-8 ($ZrB_2$, 20-vol% SiC) UHTC specimen during the second test run; connecting line serves as a visual guide only.**

473 K, the recombination coefficients rise by an order of magnitude to ~$1 \times 10^{-2}$–$2 \times 10^{-2}$. With further heating to 673 K, they increase slightly to the ~$2 \times 10^{-2}$–$3 \times 10^{-2}$ range. During the second test, the measured recombination coefficients at each of these temperatures are substantially the same as in the first test (with some experimental scatter). When the sample is heated to 923 K, we observe a steady decrease in catalytic efficiency with time. This is indicated by the downward arrow in Fig. 2, and can be seen more clearly in Fig. 4, which plots the measured recombination coefficient as a function of

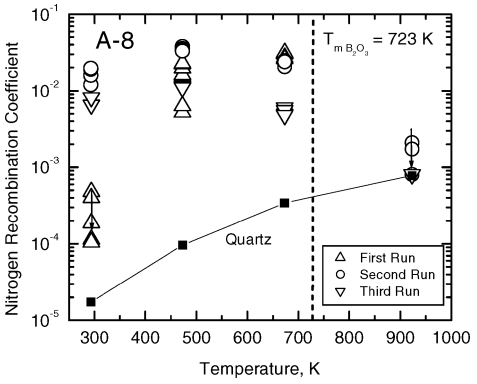


**Fig. 5 Nitrogen recombination coefficient of A-8 ($ZrB_2$, 20-vol% SiC) UHTC specimen.**

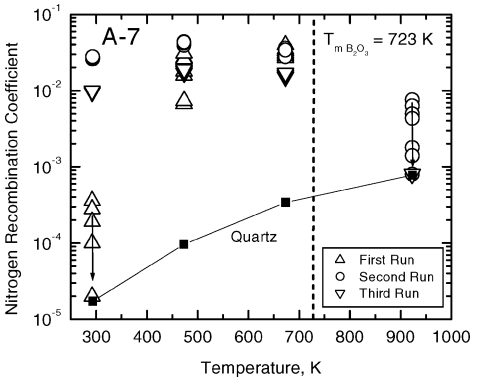


**Fig. 6 Nitrogen recombination coefficient of A-7 ($HfB_2$, 20-vol% SiC) UHTC specimen.**

time and temperature. During the third test, the sample's catalytic efficiency for O-atom recombination is drastically reduced, by one to two orders of magnitude. In fact, the recombination coefficients of the UHTC sample cannot be distinguished from those of the quartz sample tubes at the two lowest test temperatures.

The same basic phenomena are seen in Fig. 3 for the $HfB_2$, 20-vol% SiC sample: reproducible recombination coefficient values at 295, 473, and 673 K during the first two tests, a steady decrease in catalytic efficiency with time at 923 K, and lower recombination coefficient values at the lower test temperatures on retesting. The recombination coefficients are somewhat higher overall and do not decrease as much after heating at 923 K; however, the trends observed for the $HfB_2$, 20-vol% SiC sample are clearly similar to those seen for the $ZrB_2$, 20-vol% SiC sample.

### Nitrogen Surface Recombination

The measured nitrogen recombination coefficients for A-8 and A-7 are shown in Figs. 5 and 6, respectively, along with the averaged values for quartz. Distinctly different behavior is observed when the tests are conducted under dissociated nitrogen.

The initial room temperature recombination coefficients of the A-8 sample steadily decrease with time, reaching values of around $1 \times 10^{-4}$. These values increase to the $1 \times 10^{-2}$–$3 \times 10^{-2}$ range at 473 and 673 K. On the second test run, the room temperature recombination coefficients are no longer at $1 \times 10^{-4}$ but are two orders of magnitude higher. The measurements at 473 and 673 K are in reasonably good agreement with those obtained on the first run. The measurements made at 923 K show a steady decline in recombination efficiency with time, eventually making the UHTC specimens indistinguishable from the quartz side-arm tube. The third run shows recombination coefficients of order $1 \times 10^{-2}$ at room temperature, 473 K, and 673 K, in agreement with the results of the second run, though generally somewhat lower. At 923 K, the recombination coefficient is again indistinguishable from the quartz.

Similar behavior is seen for the A-7 specimen in Fig. 6, with an in initial decrease in recombination efficiency toward the quartz value during the first run, a dramatic three orders of magnitude increase in the room temperature recombination coefficient, followed by a steady decrease in catalytic efficiency at 923 K to the quartz value during the second run. The third run again shows similar, though somewhat lower values, to the second run, and recombination coefficients are indistinguishable from quartz at 923 K.

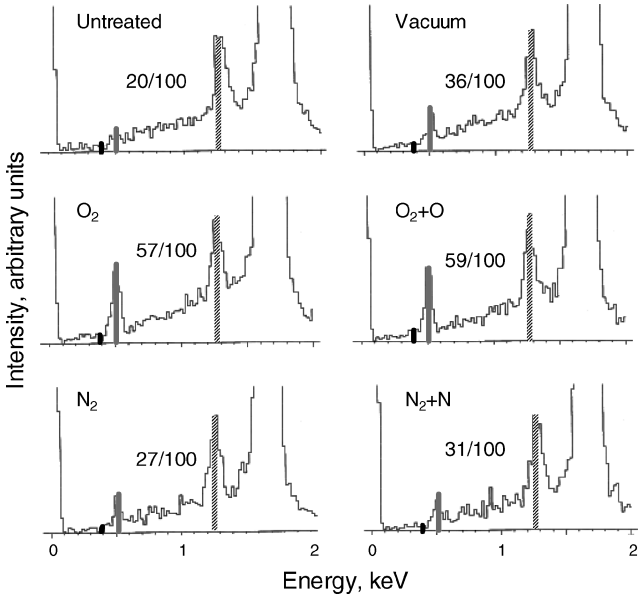


**Fig. 7 EDX analysis of run 2 A-7 ($HfB_2$, 20-vol% SiC) specimens, showing peak intensity vs x-ray energy over the range 0–2 keV: nitrogen (0.392 keV), oxygen (0.525 keV), and hafnium (1.28 keV) peaks are highlighted by bars; O/Hf peak ratios are indicated for each panel.**

### Surface Analysis

Visually, no changes were observed in any of the specimens after run 1 heating cycles. After run 2 heating cycles, a faint tarnishing could be seen on the samples exposed to vacuum and nitrogen environments, whereas a more obvious discoloration was present on the samples exposed to oxygen environments. Similar results were seen for both the A-7 and A-8 specimens. These observations are consonant with the appearances of the catalysis test specimens after testing.

The run 2 A-7 specimens were examined by the use of EDX analysis. The results are summarized in Fig. 7. The N (0.392 keV), O (0.525 keV), and Hf (1.28 keV) peaks are indicated by black, gray, and banded bars, respectively. The nitrogen peak is negligibly small for all of the different test conditions. The EDX system is not sensitive to boron, and the silicon peaks at 1.74 and 1.836 keV are present but obscured by the strong hafnium peaks at 1.645 and 1.698 keV. The approximate ratio of the O to Hf peaks is also indicated in each panel. This ratio is about 0.20 in the untreated specimen, about one and one-half times larger for the vacuum and nitrogen exposed samples, and about three times larger for the oxygen exposed samples. There are no significant differences between the discharge-on and discharge-off spectra.

Figure 8 shows XPS survey spectra for the untreated A-7 sample, along with the A-7 samples exposed to oxygen and nitrogen during discharge-on run 1 and run 2 heating cycles. The oxygen, hafnium, and carbon peaks are prominent, whereas the silicon and boron peaks are very small. No nitrogen peak is seen. The surface composition of each sample (neglecting any contribution from silicon) was calculated with standard methods and published sensitivity factors.[20] Figure 9 plots the relative surface composition for these samples. Compared to the untreated sample, the oxygen to hafnium ratio increases by approximately 35% during the $O_2 + O$ run 1 treatment, but then decreases to approximately 10% below the untreated sample during the $O_2 + O$ run 2 treatment. Similarly, during the $N_2 + N$ run 1 treatment, the oxygen to hafnium ratio increases by approximately 35% compared to the untreated sample and decreases to

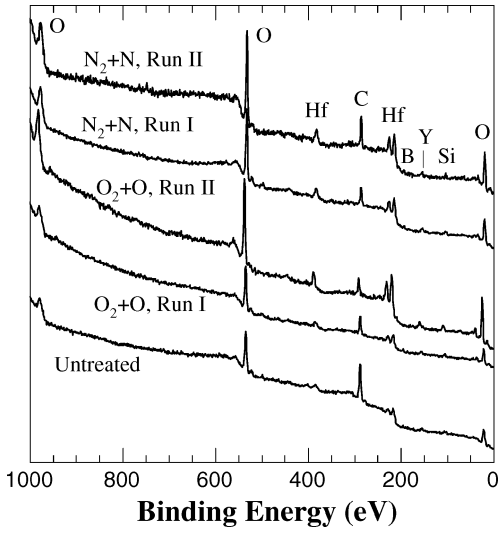


**Fig. 8 XPS survey scans of A-7 ($HfB_2$, 20-vol% SiC) specimens exposed the oxygen and nitrogen with the discharge on; spectra have been offset to enable comparison.**

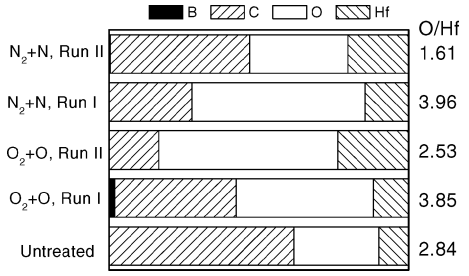


**Fig. 9 XPS determined relative surface composition of the untreated, run 1, and run 2 A-7 samples exposed to oxygen and nitrogen with the discharge on.**

approximately 40% below the untreated sample during the $N_2 + N$ run 2 treatment.

## Discussion

The maximum oxygen and nitrogen recombination coefficients, measured at 473 and 673 K before samples are heated to 923 K, are about $5 \times 10^{-2}$. A recombination coefficient of $5 \times 10^{-2}$ is similar to values measured in this same temperature range for oxidized Inconel 617, but is one to two orders of magnitude greater than typical values found for glassy silica-based coatings such as the reaction cured glass (RCG) shuttle tile coating.[21] When samples are heated to 923 K, catalytic efficiencies are seen to decrease steadily in time. Retesting of these samples reveals a lowered catalytic efficiency, in some cases indistinguishable from the quartz side-arm tube. This irreversible behavior suggests that some morphological and/or chemical changes are occurring at the sample surfaces during temperature cycling and gas exposure, even at these relatively mild environmental conditions.

Before suggesting possible scenarios for this behavior, we comment on the repeatability of the experimental technique and the accuracy of the derived recombination coefficients. For a chemically stable low catalytic efficiency material such as quartz, measurements made in rapid succession generally produce recombination coefficients that differ by less than 10%. Exceptions occur at high temperatures where the decreasing atom number density and the increasing thermal background from the furnace degrades the signal-to-noise ratio, or when initial heating or discharge operation produces transients associated with the removal of surface contaminates such as water. For materials with higher catalytic efficiency, the scatter in successive measurements is typically higher at a given temperature because more atoms are removed from the gas phase, lowering the LIF signal. However, this scatter still rarely exceeds 25%. It is evident that the systematic decreases in catalytic activity observed in successive measurements on UHTC samples heated to 923 K are not artifacts of experimental scatter. The observed changes are monotonic, large, and occurred on four different samples over the same temperature range.

The absolute accuracy of measured recombination coefficients is more problematic to evaluate. First, recombination coefficients extracted from the experimental data are coupled to the surface chemistry and gas flow assumptions used during data analysis. Because these vary with different techniques, it is safest to compare values for materials measured by the same experimental and data analysis approaches. Second, the recombination coefficient values we obtain are effective values in the sense that both the intrinsic material chemistry and the microscopic reactive surface area contribute to the measured value. We make no attempt to separate these contributions experimentally. Test samples are prepared as they would be for actual service; that is, we employ EDM and surface grinding techniques consistent with those used for the SHARP B1 and SHARP B2 flight articles. Third, when UHTC materials are tested it is likely that some recombination of atoms occurs on the ends and outer cylindrical surface of the tubular specimens, because the fit between the samples and the quartz tube inserts was not snug. Data were evaluated by the use of the inner diameter of the quartz tube inserts, which could lead to a systematic overestimation by a factor of $\sim$2. Thus, we make no claims of absolute accuracy beyond order-of-magnitude type quantification, which is sufficient to place the maximum observed UHTC catalytic efficiencies in the range typically seen for oxidized metals and from one to two orders of magnitude above the range for silica, quartz, and RCG.

We now present some possible scenarios for the transient catalytic behavior described earlier. For the oxygen-exposed samples, the results can be rationalized under the presumption of the formation of a $B_2O_3$ surface oxide. Crystalline $B_2O_3$ has a well-defined melting point of $\sim$723 K that lies above 673 K, the highest temperature that produced no irreversible changes in catalytic efficiency, and below 923 K, where steady declines in catalytic efficiency were observed. Amorphous $B_2O_3$ glass does not have a distinct melting point, but softening temperatures between $\sim$830 and 900 K have been reported.[22] The formation and melting of $B_2O_3$ could plausibly lead to lower catalytic efficiency, either by decreasing the reactive surface area as the $B_2O_3$ melts or because $B_2O_3$ is inherently less catalytic than the underlying UHTC material.

The temperature and oxygen partial pressure conditions present during catalysis testing should restrict any oxidation of SiC, $ZrB_2$, or $HfB_2$ to the passive oxidation regime where no volatile oxides are formed directly.[23,24] A very rough estimation of $B_2O_3$ oxide growth, based on the activation energy and pressure dependence of the $ZrB_2$ oxidation rate determined by Kuriakose and Margrave,[25] predicts $\sim$230 nm of $B_2O_3$ after 10 h of exposure to 923 K and 0.3 torr oxygen. The oxidation rate for SiC should be much slower, and similar estimates based on an extrapolation of the single-crystal SiC oxidation rates measured by Zheng et al.[26] predict a $\sim$3-nm-thick $SiO_2$ layer. Though dissociated oxygen can cause more rapid oxidation, this is not likely to be a significant mechanism in our experiments because the ratio of O atoms to $O_2$ molecules is less than $\sim 10^{-3}$ at the sample location in the side-arm reactor.

Support for surface oxidation under the catalysis test conditions is provided by the EDX measurements, which show a significant increase in the O/Hf ratio for the A-7 samples after exposure to oxygen and heating to 923 K. A similar increase is seen in the XPS result for the A-7 sample heated to 673 K in $O + O_2$, though the XPS results for the analogous sample heated to 923 K show a drop in this ratio. Some discrepancy between EDX and XPS trends are expected because XPS is very sensitive to surface contamination, such as adventitious hydrocarbons and surface depletion and/or enrichment of elements. EDX data are less affected by monolayer scale changes on the surface and will better reflect changes in the top micrometer or so of material.

For the nitrogen-exposed samples, the surface catalysis results are more puzzling. The initial decrease in catalytic efficiency suggests a transient period of surface reaction involving N atoms and

surface adsorbed species that tie up active sites on the surface. After the first heating cycle to 673 K, the second room temperature test reveals a much higher catalytic activity at room temperature, which is consistent with the thermal desorption of adsorbed species from the active sites, freeing them to be sites for N-atom recombination.

The irreversible reduction in catalytic efficiency at high temperature is difficult to explain in terms of nitrogen chemistry because nitride formation does not seem reasonable at these temperatures. Moreover, no nitrogen signatures were found in either the EDX or the XPS surface analysis. In principle, $B_2O_3$ should not form during these experiments, but in practice it is plausible that residual air leaks in the side-arm reactor system could admit sufficient oxygen into the test environment. The side-arm reactor is constructed of glassware joined by O-ring fittings and does not reach a base pressure below a few millitorr. EDX measurements support this view because both samples heated in a (nominal) vacuum and under nitrogen exhibit larger O/Hf ratios than the untreated specimen. If it is postulated that $B_2O_3$ is formed, then the reduction of the catalytic efficiency during the second run at 923 K could be ascribed to a similar $B_2O_3$ melting/coating phenomena as that for the oxygen catalysis experiments. This hypothesis is also consistent with the general reduction of catalytic efficiency during the third runs that occurred in the oxygen experiments.

In actual application, these materials are expected to see much higher surface temperatures and experience significant surface shear stresses. Boron oxide surface layers will not survive, both because shear forces will strip the $B_2O_3$ melt from leading edges and because $B_2O_3$ evaporation becomes significant above about 1500 K (Refs. 6, 27, and 28). However, a similar interplay between surface oxidation and surface catalytic efficiency might be anticipated at higher temperatures were silica formation and subsequent melting become significant. This elevated temperature regime (above $\sim$1500 K) cannot be accessed by the use of side-arm diffusion-tube techniques and awaits exploration with arc-jet testing.[17,29]

## Conclusions

The two major findings of this study are as follows:

1) The efficiency of $ZrB_2$/SiC and $HfB_2$/SiC composites for recombining dissociated oxygen and nitrogen can be nonnegligible between room temperature and 1000 K, with maximum observed recombination coefficients of $\sim 5 \times 10^{-2}$.

2) The catalytic efficiency of UHTC materials can be altered by interactions with the environment even at relatively low temperatures; in particular, surface oxidation appears to lower the catalytic efficiency below that of the virgin material.

For aeroconvective heating computations, we suggest that, for temperatures up to 1000 K, a constant (temperature-independent) recombination coefficient of 0.1 would be an appropriate compromise between the extreme conservative limit of 1 and the observed maximum of $5 \times 10^{-2}$. Above 1000 K, it would be advisable to use the limiting value of 1 until the true situation is explored experimentally.

## Acknowledgments

This work was supported by the Ceramics Program of the U.S. Air Force Office of Scientific Research, through Contract F49620-01-C-0026. The authors thank Sylvia Johnson and Donald Ellerby of the Thermal Protection Materials and Systems Branch at NASA Ames Research Center for helpful discussions, UHTC materials, and access to the side-arm reactor facility. Catalysis test samples were machined by Metal Samples Company (Munford, Alabama) and surface analysis samples by Ron Kell Engineering (Sunnyvale, California).

## References

[1]Upadhya, K., Yang, J.-M., and Hoffman, W. P., "Materials for Ultrahigh Temperature Structural Applications," *American Ceramic Society Bulletin*, Vol. 76, No. 12, 1997, pp. 51–56.

[2]Kaufman, L., "Boride Composites—A New Generation of Nose Cap and Leading Edge Materials for Reusable Lifting Re-Entry Systems," AIAA Paper 70-278, Feb. 1970.

[3]Clougherty, E. V., Pober, R. L., and Kaufman, L., "Synthesis of Oxidation Resistant Metal Diboride Composites," *Transactions of the Metallurgical Society of AIME*, Vol. 242, June 1968, pp. 1077–1082.

[4]Tripp, W. C., Davis, H. H., and Graham, H. C., "Effect of an SiC Addition on the Oxidation of $ZrB_2$," *Ceramic Bulletin*, Vol. 52, No. 8, 1973, pp. 612–616.

[5]Bull, J., "The Influence of SiC on the Ablation Response of Advanced Refractory Composite Materials," *19th Conference on Composite Materials and Structures*, Pt. 1, Advanced Materials Processes and Technology Information Analysis Center, Rome, NY, 1995, pp. 157–181.

[6]Metcalfe, A. G., Elsner, N. B., Allen, D. T., Wuchina, E., Opeka, M., and Opila, E., "Oxidation of Hafnium Diboride," *Electrochemical Society Proceedings*, Vol. 99-38, 1999, pp. 489–501.

[7]Talmy, I. G., Zaykoski, J. A., and Opeka, M. A., "Properties of Ceramics in the $ZrB_2$/ZrC/SiC System Prepared by Reactive Processing," *Ceramic Engineering and Science Proceedings*, Vol. 19, No. 3, 1998, pp. 104–112.

[8]Bull, J., Kolodziej, P., Salute, J., and Keese, D., "Design, Instrumentation and Preflight Testing of a Sharp Ultra-High Temperature Ceramic Nosetip," NASA TM-1998-112229, Oct. 1998.

[9]Kolodziej, P., Bull, J., Salute, J., and Keese, D. L., "First Flight Demonstration of a Sharp Ultra-High Temperature Ceramic Nosetip," NASA TM-112215, Dec. 1997.

[10]Rakich, J. V., Stewart, D. A., and Lanfranco, M. J., "Results of a Flight Experiment on the Catalytic Efficiency of the Space Shuttle Heat Shield," AIAA Paper 82-0944, June 1982.

[11]Stewart, D. A., Rakich, J. V., and Lanfranco, M. J., "Catalytic Surface Effects on Space Shuttle Thermal Protection System During Earth Entry of Flights STS-2 Through STS-5," NASA CP-2283, March 1983.

[12]Stewart, D. A., Rakich, J. V., and Chen, Y.-K., "Flight Experiment Demonstrating the Effect of Surface Catalysis on the Heating Distribution Over the Space Shuttle Heat Shield," NASA CP-3248, April 1995.

[13]Linnett, J. W., and Rahman, M. L., "Recombination of Atoms at Surfaces, Part 13—Oxygen Atoms on $Zn_xFe_{3-x}O_4$ and $Ni_xFe_{3-x}O_4$," *Transactions of the Faraday Society*, Vol. 67, 1971, pp. 191–197.

[14]Cauquot, P., Cavadias, S., and Amouroux, J., "Thermal Energy Accommodation from Oxygen Atoms Recombination on Metallic Surfaces," *Journal of Thermophysics and Heat Transfer*, Vol. 12, No. 2, 1998, pp. 206–213.

[15]Marschall, J., "Experimental Determination of Oxygen and Nitrogen Recombination Coefficients at Elevated Temperature Using Laser-Induced Fluorescence," AIAA Paper 97-3879, Aug. 1997.

[16]Sepka, S., Chen, Y.-K., Marschall, J., and Copeland, R. A., "Experimental Investigation of Surface Reactions in Carbon Monoxide and Oxygen Mixtures," *Journal of Thermophysics and Heat Transfer*, Vol. 14, No. 1, 2000, pp. 45–52.

[17]Stewart, D. A., "Determination of Surface Catalytic Efficiency for Thermal Protection Materials—Room Temperature to Their Upper Use Limit," AIAA Paper 96-1863, June 1996.

[18]Smith, W. V., "The Surface Recombination of H Atoms and OH Radicals," *Journal of Chemical Physics*, Vol. 11, March 1943, pp. 110–125.

[19]Wood, B. J., and Wise, H., "The Interaction of Atoms with Solid Surfaces," *Rarefied Gas Dynamics*, edited by L. Talbot, Academic Press, New York, 1961, pp. 51–59.

[20]Briggs, D., and Seah, M. P. (eds.) *Practical Surface Analysis by Auger and X-Ray Photoelectron Spectroscopy*, Wiley, New York, 1983, pp. 181–214.

[21]Stewart, D. A., "Surface Catalysis and Characterization of Proposed Candidate TPS for Access-to-Space Vehicles," NASA TM-112206, July 1997.

[22]Rizzo, H. F., "Oxidation of Boron at Temperatures Between 400 and 1300°C in Air," *Boron-Synthesis, Structure, and Properties*, edited by J. A. Kohn and W. F. Nye, Plenum, New York, 1968, pp. 175–189.

[23]Vaughn, W. L., and Maahs, H. G., "Active-to-Passive Transition in the Oxidation of Silicon Carbide and Silicon Nitride in Air," *Journal of the American Ceramic Society*, Vol. 73, No. 6, 1990, pp. 1540–1543.

[24]Nixon, T. D., and Cawley, J. D., "Oxidation Inhibition Mechanism in Coated Carbon–Carbon Composites," *Journal of the American Ceramic Society*, Vol. 75, No. 3, 1992, pp. 703–708.

[25]Kuriakose, A. K., and Margrave, J. L., "The Oxidation Kinetics of Zirconium Diboride and Zirconium Carbide at High Temperatures," *Journal of the Electrochemical Society*, Vol. 111, No. 7, 1964, pp. 827–831.

[26]Zheng, Z., Tressler, R. E., and Spear, K. E., "Oxidation of Single-Crystal Silicon Carbide," *Journal of the Electrochemical Society*, Vol. 137, No. 3, 1990, pp. 854–858.

[27]Singh, M., and Wiedemeier, H., "Chemical Interactions in Diboride-Reinforced Oxide-Matrix Composites," *Journal of the American Ceramic Society*, Vol. 74, No. 4, 1991, pp. 724–727.

[28]Tripp, W. C., and Graham, H. C., "Thermogravimetric Study of the Oxidation of $ZrB_2$ in the Temperature Range of 800 to 1500°C," *Journal of the Electrochemical Society*, Vol. 118, No. 7, 1971, pp. 1195–1199.

[29]Stewart, D. A., Chen, Y.-K., Bamford, D. J., and Romanovsky, A. B., "Predicting Material Surface Catalytic Efficiency Using Arc-Jet Tests," AIAA Paper 95-2013, June 1995.

B. Hassan
*Associate Editor*